Size and Structure Dependence of Electronic States in Thiolate- Protected Gold Nanoclusters of Au 25 (SR) 18 , Au 38 (SR) 24 , and Au 144 (SR) 60

ARTICLE *in* THE JOURNAL OF PHYSICAL CHEMISTRY C · FEBRUARY 2013

Impact Factor: 4.77 · DOI: 10.1021/jp400785f

6 AUTHORS, INCLUDING:

Masahiro Shibuta
Keio University
20 PUBLICATIONS **100** CITATIONS
SEE PROFILE

Yuichi Negishi
Tokyo University of Science
89 PUBLICATIONS **4,455** CITATIONS
SEE PROFILE

Toyoaki Eguchi
Keio University
85 PUBLICATIONS **858** CITATIONS
SEE PROFILE

THE JOURNAL OF PHYSICAL CHEMISTRY C

Article

pubs.acs.org/JPCC

Size and Structure Dependence of Electronic States in Thiolate-Protected Gold Nanoclusters of $Au_{25}(SR)_{18}$, $Au_{38}(SR)_{24}$, and $Au_{144}(SR)_{60}$

Tsutomu Ohta,[†] Masahiro Shibuta,[†,‡] Hironori Tsunoyama,[†,‡] Yuichi Negishi,[§] Toyoaki Eguchi,[†,‡] and Atsushi Nakajima*[,†,‡]

[†]Department of Chemistry, Faculty of Science and Technology, Keio University, 3-14-1 Hiyoshi, Kohoku-ku, Yokohama 223-8522, Japan

[‡]Nakajima Designer Nanocluster Assembly Project, ERATO, JST, 3-2-1 Sakado, Takatsu-ku, Kawasaki 213-0012, Japan

[§]Department of Applied Chemistry, Faculty of Science, Tokyo University of Science, 1-3 Kagurazaka, Shinjuku-ku, Tokyo 162-8601, Japan

ABSTRACT: The electronic states of three different sizes of compositionally precise thiolate-protected gold nanoclusters, $Au_{25}(SR)_{18}$, $Au_{38}(SR)_{24}$, and $Au_{144}(SR)_{60}$ (R = $C_{12}H_{25}$), have been evaluated by X-ray photoemission spectroscopy. The Au 4*f* core-levels of the nanoclusters are well reproduced by two spectral components derived from centered core-Au and positively charged shell-Au atoms, the numbers of which are determined based on the atomic structures of the nanoclusters. The spin−orbit splitting of Au $5d_{5/2}$ and $5d_{3/2}$ in the valence band becomes narrower than that for bulk Au, depending on the cluster size, which is quantitatively characterized by a reduction in the average coordination number of Au. The Au 5*d* valence-band spectra also show that the charge reorganization of 5*d* electrons induced by interaction with thiol molecules is more significant for the $5d_{5/2}$ than the $5d_{3/2}$ orbital.

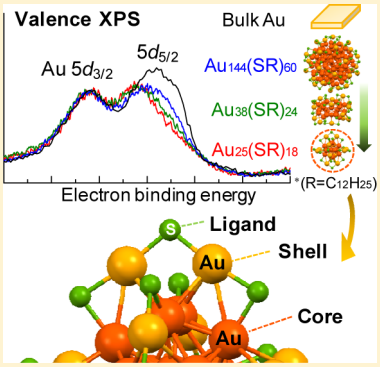

1. INTRODUCTION

Metal nanoparticles (NPs) and nanoclusters have attracted a great deal of attention because of their potential application to magnetic, optical, electronic devices, and catalysts.[1,2] One of the most important issue of these nanoclusters is that their properties are controllable not only by their constituent elements, but also by their sizes. Among the metal NPs, gold NPs protected by thiolates have been studied most extensively with regard to synthesis methods, size-dependent properties, and functionalization,[3−8] which is relevant to thiolate-protected gold surfaces and interfaces, including self-assembled monolayers of organic molecules on gold.[9,10] Thiolate-protected Au (Au:SR) NPs have been successfully synthesized with high monodispersity,[11−21] and various of their properties, such as optical,[11−15] electronic,[11,16] magnetic,[17−19] and catalytic,[20,21] have been investigated, none of which appear in the bulk form. In order to reveal the origin of the size specific properties, it is crucial to investigate the size dependence of their electronic structures. Although systematic studies of the electronic structure of Au:SR NPs have revealed a size dependence of the charge state of the Au atoms, the valence band energy levels, and the hole density in the Au 5*d* band,[22−28] the origin of these size-specific properties are still under debate, which is likely ascribable to a poor understanding of the correlation between their geometric and electronic structures.

Recently, Au:SR nanoclusters with a *well-defined* "*size*" and "*chemical composition*" have been successfully synthesized, and as a result, a series of stable nanoclusters, so-called magic-number clusters have been isolated.[5−8] Among them, the geometric structures of $[Au_{25}(SR)_{18}]^-$, $Au_{38}(SR)_{24}$, and $Au_{102}(SR)_{44}$ nanoclusters were identified by single-crystal X-ray diffraction (XRD).[29−32] $Au_{144}(SR)_{60}$ is the second most common of the magic-number Au:SR nanoclusters. Although the single-crystal XRD analysis of $Au_{144}(SR)_{60}$ has not been reported yet, there are extensive discussion about its geometric structure based on the combination of various experiments and quantum chemical calculations.[33] These achievements enable us to establish a correlation between electronic and geometric structures at the atomic level. Indeed, some of the properties of Au:SR nanoclusters, such as their magneto-optical and photoluminescence properties, have been reconsidered based on this geometric model.[5] In this study, by using X-ray photoelectron spectroscopy (XPS), we have studied the electronic states of three sizes of Au:SR nanoclusters having well-established geometric structures, $[Au_{25}(SR)_{18}]^-$,[29,30] $Au_{38}(SR)_{24}$,[31] and $Au_{144}(SR)_{60}$[33] (R = $C_{12}H_{25}$), each with a single atomic composition [see structural models in Figure 1(a)−(c)]; their size and structure dependences are discussed from the atomic viewpoint.

Received: January 23, 2013
Revised: January 29, 2013
Published: February 11, 2013

   dx.doi.org/10.1021/jp400785f | *J. Phys. Chem. C* 2013, 117, 3674−3679

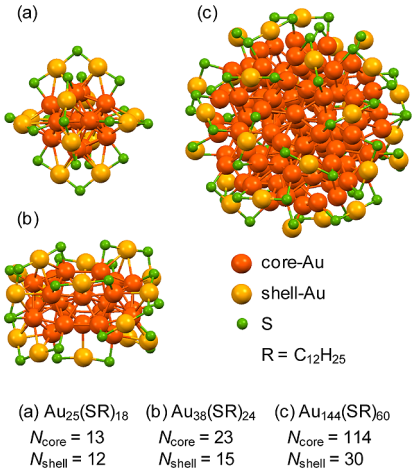

Figure 1. Geometric structures of $Au_{25}(SR)_{18}$, $Au_{38}(SR)_{24}$, and $Au_{144}(SR)_{60}$. Red, orange, and green spheres represent core-Au, shell-Au, and S atoms, respectively. The R groups are omitted for simplicity. N_{core} and N_{shell} are numbers of core-Au and shell-Au atoms, respectively.

2. EXPERIMENTAL SECTION

Single composition Au:SR nanoclusters of $[Au_{25}(SR)_{18}]^-$ (abbreviated as $Au_{25}(SR)_{18}$), $Au_{38}(SR)_{24}$, and $Au_{144}(SR)_{60}$ have been synthesized by the Brust method[34] with a little modification. Isolation of each nanocluster was confirmed by matrix assisted laser desorption/ionization mass spectrometry and ultraviolet/visible absorption spectroscopy based on the reported spectra.[35,36] The Langmuir−Blodgett (LB) method has been employed to fabricate uniform and monolayer films of Au:SR nanoclusters on a highly oriented pyrolytic graphite (HOPG) substrate which is suitable to analyze the valence band structures of the Au nanoclusters supported on the substrate, because the density of state of HOPG near the Fermi level is very low and nearly constant. The HOPG substrate was cleaved in air and heated up to 700 K in ultra high vacuum (UHV) for 20 h before use. To prepare LB films, nanoclusters of $Au_{25}(SR)_{18}$, $Au_{38}(SR)_{24}$, and $Au_{144}(SR)_{60}$ were dissolved in 56 μM dichloromethane, 20 μM chloroform, and 25 μM chloroform, respectively. These solutions were carefully spread onto ultrapure water in a trough with subsequent evaporation of solvent and compression of the nanocluster into a film (USI Corp., FSD-50). The cleaned HOPG substrate was carefully contacted to the monolayer film of nanoclusters at a surface pressure of 10 mN/m and immediately introduced into an UHV chamber through a load lock.

All XPS measurements were performed under UHV condition with a base pressure of $<2 \times 10^{-8}$ Pa. The X-ray source using the Mg $K\alpha$ line ($h\nu$ = 1253.6 eV) was irradiated on the sample at an incident angle of 45°. Photoelectrons emitted at 45° from the surface normal were collected by a hemispherical electron analyzer (VG Scienta, R-3000). The samples were well connected to ground to avoid a sample charging as a result of electron emission during X-ray irradiation. It was carefully verified that there were no effects of X-ray irradiation on the XPS spectra for all samples.

3. RESULTS AND DISCUSSION

3.1. Core-Level XPS Spectra for Au 4*f* and S 2*p*. Core-level XPS spectra for the Au 4*f* and S 2*p* levels were measured and are shown in Figure 2. As a reference, the XPS spectrum for Au 4*f* emission from an Au(111) surface cleaned in UHV has been measured, and is shown at the top of Figure 2(a).

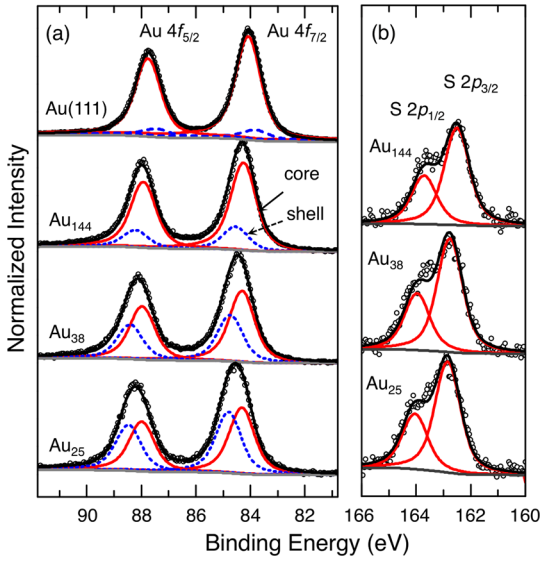

Figure 2. (a) Au 4*f* and (b) S 2*p* XPS spectra of the three nanoclusters. Solid- and broken-lines in Au 4*f* spectra represent the component derived from core-Au and shell-Au, respectively. The Au 4*f* spectra of an Au(111) clean surface is also shown for reference, in which solid- and broken-lines also represent the bulk- and surface-components, respectively.

With a decrease in the cluster size, the Au 4*f* spectra show an energy shift toward the higher binding-energy side and a peak broadening relative to that of Au(111). In order to evaluate the electronic states of the three different sizes of Au:SR nanoclusters, the XPS spectrum of Au(111) has been first analyzed to evaluate the spectral parameters in this study, based on previous X-ray photoemission studies.[24,25,37] A Shirley background was subtracted from the spectra before analysis, and the Au(111) spectrum was deconvoluted into two components, the bulk (solid lines) and surface (broken lines) with an energy separation of 0.28 eV. Each peak component was described by a convolution of a Doniach−Sunjic line shape with a Gaussian to represent the instrumental and photon energy broadening (Γ_G). This Doniach−Sunjic line shape is characterized by a Lorentzian due to the lifetime broadening (Γ_L) and the singularity index (α). From the peak analysis, Γ_G, Γ_L, and α have been evaluated to be 0.75, 0.56, and 0.02, respectively, for the Au 4*f* spectrum. The separation between the spin−orbit splitting peaks of Au $4f_{7/2}$ and Au $4f_{5/2}$ was found to be 3.67 eV with a branching ratio of 4:3. These parameters were used for the peak analysis of Au 4*f* spectra for the Au:SR nanoclusters.

In the spectral analysis of the Au:SR nanoclusters, it is reasonable to suppose that their Au 4*f* spectra are represented by two components originating from core- and shell-Au atoms,[24,25] because the numbers of core- and shell-Au atoms can be clearly counted on the basis of the structural models shown in Figure 1(a)−(c). Namely, $Au_{144}(SR)_{60}$, $Au_{38}(SR)_{24}$, and $Au_{25}(SR)_{18}$ have a common motif and consist of two components; bulk-like Au core and molecular-like shell layer of $-S(R)-[Au-S(R)-]_n$ oligomers with different length (n = 1 and 2). After deconvolution has been performed by changing the energy position of the core and shell components using the

dx.doi.org/10.1021/jp400785f | J. Phys. Chem. C 2013, 117, 3674−3679

Γ_G, Γ_L, and α values mentioned above, the Au 4*f* spectra of the Au:SR nanoclusters have been separated clearly into two components, as shown in Figure 2(a), where the solid- and dotted-lines represent the core- and shell-Au atoms components, respectively. It is noted that their intensity ratio is fixed to the value of N_{shell}/N_{core} calculated from the number of core- and shell-Au atoms (N_{core} and N_{shell}), as shown in Figure 1. However, all of the S 2*p* spectra shown in Figure 2(b) can be fitted well by a single component of S $2p_{3/2}$ and $2p_{1/2}$ signals with a common peak width (Γ_G = 0.75 eV and Γ_L = 0.58 eV), energy separation (1.20 eV) and branching ratio (2:1). The results support the contention that the present samples are composed of single-composition nanoclusters having the previously reported atomic structures with no oxidized or unreacted ligands. The parameters obtained from the peak analysis are listed in Table 1.

Table 1. Energy Positions of Au $4f_{7/2}$ and S $2p_{3/2}$ Determined by the Peak Analysis[a]

	N_{shell}/N_{core}	Au $4f_{7/2(core)}$ (eV)	Au $4f_{7/2(shell)}$ (eV)	$\Delta 4f$ (eV)	S $2p_{3/2}$ (eV)
Au(111)		84.08			
$Au_{144}(SR)_{60}$	0.263	84.25	84.52	0.27	162.5
$Au_{38}(SR)_{24}$	0.652	84.30	84.73	0.43	162.8
$Au_{25}(SR)_{18}$	0.923	84.30	84.79	0.49	162.9

[a]Intensity ratios of shell to bulk component (N_{shell}/N_{core}), Au $4f_{7/2}$ energy position of core-Au ($4f_{7/2(core)}$) and shell-Au ($4f_{7/2(shell)}$) and their energy difference ($\Delta 4f$).

The fitting result for Au 4*f* spectra shows that, for all of the nanoclusters, the Au shell component has a larger binding energy (~0.5 eV) than that of the core, which is consistent with previous studies on monodispersed Au NPs.[23−25] This indicates that core- and shell-Au atoms are different in chemical states. The different chemical states of these two Au species probably originate from the different number of thiolates ligated to Au atoms; the shell-Au atom is ligated by two thiolates whereas the core atom is ligated by one thiolate or none. As a result of charge transfer from Au to thiolate due to more electronegative nature of sulfur, the shell component is shifted to higher binding energy than core component. The difference of the chemical shift of Au 4*f* between the core and shell atoms ($\Delta 4f$) slightly increases with a reduction in the cluster size, which is similar to that in previous studies.[23−25] The result suggests that the surrounding thiolate sulfur atoms more effectively extract electron from shell-Au atoms rather than from core-Au atoms.

Furthermore, the energy positions of both core and shell components in the Au 4*f* spectra shift toward the high binding energy side relative to that of the bulk Au(111) on reducing the cluster size. A similar energy shift to the higher binding energy can be seen in the S 2*p* spectra. If the energy shift is caused by the charge transfer from Au to S discussed above, Au 4*f* and S 2*p* spectra should shift in opposite directions each other. Therefore, it can be considered that the observed energy shift is mainly attributed to the effect of a positive charge left to a nanocluster immediately after photoemission, so-called the final-state effect.[38,39] When the exciting light emits a photoelectron, the photohole left behind in the nanoclusters within the time scale of the photoemission process lowers the kinetic energy of photoelectrons through the Coulomb interaction, which results in the apparent energy shift to higher binding energy. The final-state effect would play a significant role in the present Au:SR nanoclusters supported on the substrates because of the weak coupling between the nanoclusters and the substrates through the thiolate molecules, and become more prominent for smaller clusters, as shown in the present result. It makes it difficult to discuss the size dependence of the absolute chemical shift both in Au and S atoms.

3.2. Valence-Band XPS Spectra for Au 5*d*. Next, the valence electronic states of the Au:SR nanoclusters have been evaluated. It is noteworthy that photoelectrons for Au are derived from a kind of buried surface beneath the alkyl chain layer, because Au atoms are surrounded by alkyl chains for thiolate-protected Au nanoclusters. In general, the kinetic energies of photoelectrons in the ultraviolet photoelectron spectroscopy (UPS) measurements are several tens of eV, which is around the minimum point of the universal curve;[40,41] the probe depth of the UPS experiments is too short to provide proper information on valence electronic states. In contrast to UPS, XPS can probe electronic states for Au atoms because photoelectrons are emitted by several hundred eV photon in XPS; the photoelectrons from buried surface can be involved more efficiently.

Figure 3(a) shows Au 5*d* valence-band XPS spectra of the Au:SR nanoclusters and the Au(111) clean surface. Two components originating from $5d_{3/2}$ and $5d_{5/2}$ levels split by a spin−orbit interaction are clearly visible in all spectra, and the apparent spin−orbit splitting width $\Delta 5d$ decreased on reducing the cluster size, exhibiting a similar tendency to that reported for monodispersed Au NPs.[23−27] Size dependent electronic properties of monodispersed Au NPs have been studied by changing the mean diameter in the range from 1.6 to 5.2 nm,[24−27] while the nanoclusters examined in this study are smaller in size, about 1.6 nm, 1.3 nm, and 1.0 nm for $Au_{144}(SR)_{60}$, $Au_{38}(SR)_{24}$, and $Au_{25}(SR)_{18}$, respectively.[42]

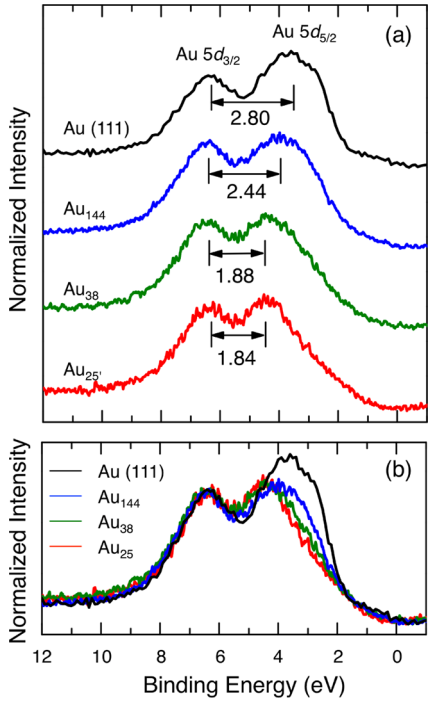

Figure 3. (a) The valence band XPS spectra of various Au nanoclusters and the Au(111) clean surface. Apparent spin−orbit splitting widths ($\Delta 5d$) as marked are shown. (b) Overlapped spectra normalized to the Au $5d_{3/2}$ intensity.

dx.doi.org/10.1021/jp400785f | J. Phys. Chem. C 2013, 117, 3674−3679

MacDonald and co-workers have studied the size-dependent nature of bonding in these three nanoclusters from the X-ray absorption near-edge structure (XANES) analysis, and also reported about the comparison between the valence band XPS for bulk Au and $Au_{144}(SR)_{60}$ but not that for $Au_{38}(SR)_{24}$ and $Au_{25}(SR)_{18}$.[23] As can be seen in Figure 3(a), the $\Delta 5d$ of the $Au_{144}(SR)_{60}$ and $Au_{38}(SR)_{24}$ nanoclusters show the systematic narrowing of $\Delta 5d$ as expected from their smaller size compare to the bulk, but the $\Delta 5d$ of $Au_{25}(SR)_{18}$ is very close to that of $Au_{38}(SR)_{24}$, although the number of Au atoms and the sizes of clusters are different. It has been established that the Au *d*-bandwidth and apparent spin−orbit splitting become narrower as the coordination number (CN) of the nearest Au atom decreases.[43,44] In the previous reports for Au NPs, the CNs were estimated from the size of the NPs using an equation proposed by Pirkkalainen and Serimaa,[45] although the CN depends on the geometric structure, not on the size. Since here single-composition nanoclusters having well-established geometric structures have been used as samples,[29,31,33] it is possible to determine the average coordination number (ACN) based on their geometric structures as shown in Figure 4. The ACN is obtained by weighting the CN of each nonequivalent atom of the clusters by the number of atoms having the same CN. The

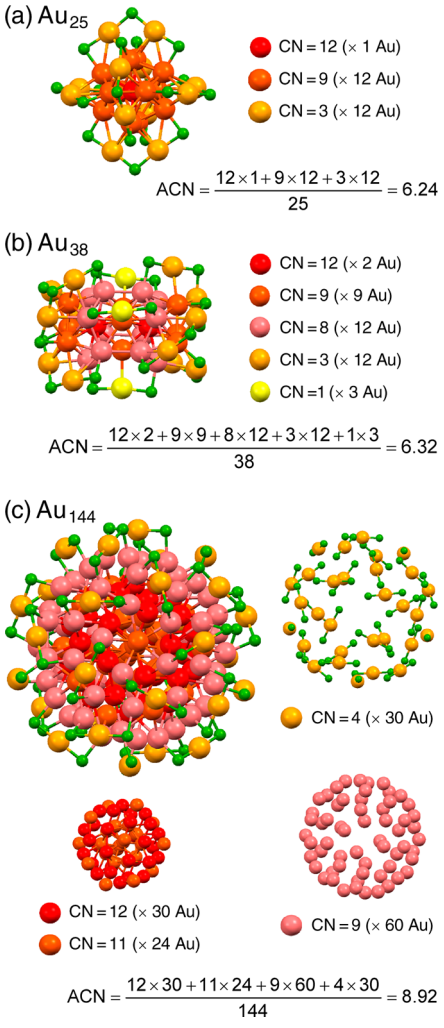

Figure 4. Calculations of ACN for (a) $[Au_{25}(SR)_{18}]^-$, (b) $Au_{38}(SR)_{24}$, and (c) $Au_{144}(SR)_{60}$. The cluster models for (a), (b), and (c) are taken from crystal structures in refs 29, 31, and 33, respectively.

ACNs of thiol-protected Au nanoclusters of $Au_{25}(SR)_{18}$, $Au_{38}(SR)_{24}$, and $Au_{144}(SR)_{60}$ have been calculated to be 6.24, 6.32, and 8.92 based on their structural model.[29,31,33] The first coordination shell distance is defined as 0.29−0.32 nm, which is slightly larger than the nearest-neighbor distance of bulk Au (0.288 nm). It is found that $Au_{25}(SR)_{18}$ and $Au_{38}(SR)_{24}$ have nearly the same ACN in spite of their difference in size, which is quite consistent with the obtained $\Delta 5d$ value. The result clearly indicates that $\Delta 5d$ of nanocluster depends not on size but rather on ACN.

It should be noted that the intensity of the Au $5d_{5/2}$ component relative to that of Au $5d_{3/2}$ obviously decreased with a decrease in the cluster size, which is clearly seen in superimposed spectra normalized to the maxima of the Au $5d_{3/2}$ shown in Figure 3(b). There have been reports on a decrease of the 5*d*-electron or an increase in that of 5*d*-hole with reducing the size of Au:SR NPs based on XANES measurement on the Au L_3-edge, from which it is possible to probe the unoccupied densities of 5*d* state just above the Fermi level arising from *s*-*d* hybridization in Au.[23] Zhang and Sham have estimated the contribution of $5d_{5/2}$ and $5d_{3/2}$ to the *d*-hole redistribution by measuring the XANES of Au:SR NPs at the L_3 and L_2 edges, which are associated with a dipole transition from $2p_{3/2}$ to $5d_{5/2,3/2}$ and from $2p_{1/2}$ to $5d_{3/2}$, respectively, and they concluded that the holes in the $5d_{3/2}$ orbitals show a more significant change than that of the $5d_{5/2}$.[28] Ohyama et al., however, have pointed out that the Au L_3- and L_2-edge XANES spectra reflected not only the electronic properties of the Au NPs themselves, but also the large scattering intensity of the Au−S pair, which is more significant in the L_2-edge.[46] Therefore, the XANES spectra cannot provide straightforward information to quantitatively evaluate the contribution of $5d_{5/2}$ and $5d_{3/2}$.

Alternatively, our XPS measurement directly reveals that the decrement of the Au 5*d* electron preferentially occurs in the $5d_{5/2}$ orbital: The electron depletion in the Au 5*d* band becomes significant as the cluster size decreases, as shown in Figure 3(b). This can be explained by the ratio of Au atoms to S atoms ligated. As pointed out by Venkataraman and co-workers,[47] it is reasonable that the interaction between Au and S atoms involves electron donation from the S lone pair to Au 6*s* and a back-donation from Au 5*d* to S states, but it seems that an electron accepting part should be discussed in detail. In theoretical calculations for ligand-protected $Au_{102}(SC_7O_2H_5)_{44}$ clusters,[48] the Au atoms in the outermost layer show a small but distinct positive mean charge, and DOS for Au 5*d* in the outermost layer is smaller than those in the inner layers. Furthermore, for density of states projected on local atomic basis (PLDOS) for S atoms of thiolate-protected $Au_{25}(SR)_{18}$ and $Au_{38}(SR)_{24}$ clusters,[49,50] theoretical calculations show that their PLDOS for S 3*p* are distributed widely in the range from −7 to 0 eV. Our result clearly shows that a substantial charge transfer takes place particularly in the outermost Au layer when thiols interact with an Au atom. Since the electronegativity of an S atom is slightly larger than that of an Au atom, it is likely that a charge transfer from Au to S occurs in the Au $5d_{5/2}$ orbital rather than in the Au $5d_{3/2}$. Since the $5d_{5/2}$ orbital is less stable than $5d_{3/2}$, it seems reasonable that the $5d_{5/2}$ orbital is more responsible for metal−ligand binding.

The electronic structures of $Au_{25}(SR)_{18}$[30,51−54] and $Au_{38}(SR)_{24}$[50,55,56] clusters have been extensively discussed based on theoretical calculation. The calculations based on density functional theory have reveal that the *d*-band of

dx.doi.org/10.1021/jp400785f | J. Phys. Chem. C 2013, 117, 3674−3679

$Au_{25}(SR)_{18}$, which is mostly composed of Au 5*d* atomic orbitals, is distributed in narrower energy range and have a less component at lower binding energy compare to that of $Au_{38}(SR)_{24}$.[30,55] A similar tendency has also been reported through the comparison of $Au_{25}(SR)_{18}$ and $Au_{19}(SR)_{13}$,[54] which reveals that the *d* bandwidth of core-Au atoms becomes narrower with a decreasing number of atoms, whereas that of shell-Au atom is almost unchanged. These results are quite consistent with our experimental findings indicating preferential electron depletion at the lower binding energy side, as shown in Figure 3(b).

4. CONCLUSIONS

We have systematically investigated the electronic states of Au:SR magic-number clusters of various sizes using XPS. The Au 4*f* and S 2*p* core-level spectra of each cluster have been interpreted in a manner consistent with their geometric structures. We have clearly demonstrated the size- and structure-dependent change in the valence electronic states. These findings will be useful in developing a deeper understanding of the relations between geometric and electronic structures of other ligand-protected metal nanoclusters.

AUTHOR INFORMATION

Corresponding Author

*Fax: +81-45-566-1697; e-mail: nakajima@chem.keio.ac.jp.

Notes

The authors declare no competing financial interest.

ACKNOWLEDGMENTS

We wish to thank Prof. Yasuaki Einaga and Dr. Takashi Yamamoto for their help in preparing the LB film. This work was partly supported by the MEXT-Supported Program for the Strategic Research Foundation at Private Universities, 2009-2013.

REFERENCES

(1) Haberland, H. *Clusters of Atoms and Molecules: Theory, Experiment, and Clusters of Atoms*; Springer-Verlag: Berlin, 1994.
(2) Schmid, G. *Clusters and Colloids: From Theory to Applications*; Wiley-VCH: Weinheim, 1994.
(3) Templeton, A. C.; Wuelfing, W. P.; Murray, R. W. Monolayer-Protected Cluster Molecules. *Acc. Chem. Res.* **2000**, *33*, 27−36.
(4) Whetten, R. L.; Khoury, J. T.; Alvarez, M. M.; Murthy, S.; Vezmar, I.; Wang, Z. L.; Stephens, P. W.; Cleveland, C. L.; Luedtke, W. D.; Landman, U. Nanocrystal Gold Molecules. *Adv. Mater.* **1996**, *8*, 428−433.
(5) Tsukuda, T. Toward an Atomic-Level Understanding of Size-Specific Properties of Protected and Stabilized Gold Clusters. *Bull. Chem. Soc. Jpn.* **2012**, *85*, 151−168.
(6) Jin, R. Quantum Sized, Thiolate-Protected Gold Nanoclusters. *Nanoscale* **2010**, *2*, 343−362.
(7) Parker, J. F.; Fields-Zinna, C. A.; Murray, R. W. The Story of a Monodisperse Gold Nanoparticle: $Au_{25}L_{18}$. *Acc. Chem. Res.* **2010**, *43*, 1289−1296.
(8) Häkkinen, H. Atomic and Electronic Structure of Gold Clusters: Understanding Flakes, Cages and Superatoms from Simple Concepts. *Chem. Soc. Rev.* **2008**, *37*, 1847−1859.
(9) Walter, M.; Akola, J.; Lopez-Acevedo, O.; Jadzinsky, P. D.; Calero, G.; Ackerson, C. J.; Whetten, R. L.; Grönbeck, H.; Häkkinen, H. A Unified View of Ligand-Protected Gold Clusters as Superatom Complexes. *Proc. Natl. Acad. Sci. U.S.A.* **2008**, *105*, 9157−9162.
(10) Häkkinen, H. The Gold−Sulfur Interface at the Nanoscale. *Nat. Chem.* **2012**, *4*, 443−455.
(11) Negishi, Y.; Nobusada, K.; Tsukuda, T. Glutathione-Protected Gold Clusters Revisited: Bridging the Gap between Gold(I)−Thiolate Complexes and Thiolate-Protected Gold Nanocrystals. *J. Am. Chem. Soc.* **2005**, *127*, 5261−5270.
(12) Chen, S.; Ingram, R. S.; Hostetler, M. J.; Pietron, J. J.; Murray, R. W.; Schaaff, T. G.; Khoury, J. T.; Alvarez, M. M.; Whetten, R. L. Gold Nanoelectrodes of Varied Size: Transition to Molecule-Like Charging. *Science* **1998**, *280*, 2098−2101.
(13) Knoppe, S.; Kothalawala, N.; Jupally, V. R.; Dass, A.; Bürgi, T. Ligand Dependence of the Synthetic Approach and Chiroptical Properties of a Magic Cluster Protected with a Bicyclic Chiral Thiolate. *Chem. Commun.* **2012**, *48*, 4630−4632.
(14) Yao, H.; Miki, K.; Nishida, N.; Sasaki, A.; Kimura, K. Large Optical Activity of Gold Nanocluster Enantiomers Induced by a Pair of Optically Active Penicillamines. *J. Am. Chem. Soc.* **2005**, *127*, 15536−15543.
(15) Schaaff, T. G.; Knight, G.; Shafigullin, M. N.; Borkman, R. F.; Whetten, R. L. Isolation and Selected Properties of a 10.4 kDa Gold:Glutathione Cluster Compound. *J. Phys. Chem. B* **1998**, *102*, 10643−10646.
(16) Laaksonen, T.; V. Ruiz, V.; Liljeroth, P.; Quinn, B. M. Quantised Charging of Monolayer-Protected Nanoparticles. *Chem. Soc. Rev.* **2008**, *37*, 1836−1846.
(17) Negishi, Y.; Tsunoyama, H.; Suzuki, M.; Kawamura, N.; Matsushita, M. M.; Maruyama, K.; Sugawara, T.; Yokoyama, T.; Tsukuda, T. X-ray Magnetic Circular Dichroism of Size-Selected, Thiolated Gold Clusters. *J. Am. Chem. Soc.* **2006**, *128*, 12034−12035.
(18) Crespo, P.; Litrán, R.; Rojas, T. C.; Multigner, M.; Fuente, J. M. d. l.; Sánchez-López, J. C.; García, M. A.; Hernando, A.; Penadés, S.; Fernández, A. Permanent Magnetism, Magnetic Anisotropy, and Hysteresis of Thiol-Capped Gold Nanoparticles. *Phys. Rev. Lett.* **2004**, *93*, 087204.
(19) Hori, H.; Yamamoto, Y.; Iwamoto, T.; Miura, T.; Teranishi, T.; Miyake, M. Diameter Dependence of Ferromagnetic Spin Moment in Au Nanocrystals. *Phys. Rev. B* **2004**, *69*, 174411.
(20) Zhu, Y.; Qian, H.; Drake, B. A.; Jin, R. Atomically Precise $Au_{25}(SR)_{18}$ Nanoparticles as Catalysts for the Selective Hydrogenation of α,β-Unsaturated Ketones and Aldehydes. *Angew. Chem., Int. Ed.* **2010**, *49*, 1295−1298.
(21) Zhu, Y.; Wu, Z.; Gayathri, C.; Qian, H.; Gil, R. R.; Jin, R. Exploring Stereoselectivity of Au_{25} Nanoparticle Catalyst for Hydrogenation of Cyclic Ketone. *J. Catal.* **2010**, *271*, 155−160.
(22) MacDonald, M. A.; Zhang, P.; Chen, N.; Qian, H.; Jin, R. Solution-Phase Structure and Bonding of $Au_{38}(SR)_{24}$ Nanoclusters from X-ray Absorption Spectroscopy. *J. Phys. Chem. C* **2011**, *115*, 65−69.
(23) MacDonald, M. A.; Zhang, P.; Qian, H.; Jin, R. Site-Specific and Size-Dependent Bonding of Compositionally Precise Gold−Thiolate Nanoparticles from X-ray Spectroscopy. *J. Phys. Chem. Lett.* **2010**, *1*, 1821−1825.
(24) Tanaka, A.; Takeda, Y.; Imamura, M.; Sato, S. Dynamic Final-State Effect on the Au 4*f* Core-Level Photoemission of Dodecanethiolate-Passivated Au Nanoparticles on Graphite Substrates. *Phys. Rev. B* **2003**, *68*, 195415.
(25) Tanaka, A.; Takeda, Y.; Nagasawa, T.; Takahashi, K. Chemical States of Dodecanethiolate-Passivated Au Nanoparticles: Synchrotron-Radiation Photoelectron Spectroscopy. *Solid State Commun.* **2003**, *126*, 191−196.
(26) Yiu, Y. M.; Zhang, P.; Sham, T. K. The Electronic Properties and L_3 XANES of Au and Nano-Au. *Technical Proceedings of the 2003 Nanotechnology Conference and Trade Show Nanotechnology* **2003**, *3*, 183−186.
(27) Zhang, P.; Sham, T. K.; X-Ray, T. K. Studies of the Structure and Electronic Behavior of Alkanethiolate-Capped Gold Nanoparticles: The Interplay of Size and Surface Effects. *Phys. Rev. Lett.* **2003**, *90*, 245501.
(28) Zhang, P.; T. K. Sham, T. K. Tuning the Electronic Behavior of Au Nanoparticles with Capping Molecules. *Appl. Phys. Lett.* **2002**, *81*, 736−739.

(29) Heaven, N. W.; Dass, A.; White, P. S.; Holt, K. M.; Murray, R. W. Crystal Structure of the Gold Nanoparticle $[N(C_8H_{17})_4][Au_{25}(SCH_2CH_2Ph)_{18}]$. *J. Am. Chem. Soc.* **2008**, *130*, 3754−3755.
(30) Zhu, M.; Aikens, C. M.; Hollander, F. J.; Schatz, G. C.; Jin, R. Correlating the Crystal Structure of A Thiol-Protected Au_{25} Cluster and Optical Properties. *J. Am. Chem. Soc.* **2008**, *130*, 5883−5885.
(31) Qian, H.; Eckenhoff, W. T.; Zhu, Y.; Pintauer, T.; Jin, R. Total Structure Determination of Thiolate-Protected Au_{38} Nanoparticles. *J. Am. Chem. Soc.* **2010**, *132*, 8280−8281.
(32) Jadzinsky, P. D.; Calero, G.; Ackerson, C. J.; Bushnell, D. A.; Kornberg, R. D. Structure of a Thiol Monolayer−Protected Gold Nanoparticle at 1.1 Å Resolution. *Science* **2007**, *318*, 430−433.
(33) Lopez-Acevedo, O.; Akola, J.; Whetten, R. L.; Grnbeck, H.; Häkkinen, H. Structure and Bonding in the Ubiquitous Icosahedral Metallic Gold Cluster $Au_{144}(SR)_{60}$. *J. Phys. Chem. C* **2009**, *113*, 5035−5038.
(34) Brust, M.; Walker, M.; Bethell, D.; Schiffrin, D. J.; Whyman, R. Synthesis of Thiol-Derivatised Gold Nanoparticles in a Two-Phase Liquid−Liquid System. *J. Chem. Soc., Chem. Comm.* **1994**, 801−802.
(35) Negishi, Y.; Chaki, N. K.; Shichibu, Y.; Whetten, R. L.; Tsukuda, T. Origin of Magic Stability of Thiolated Gold Clusters: A Case Study on $Au_{25}(SC_6H_{13})_{18}$. *J. Am. Chem. Soc.* **2007**, *129*, 11322−11323.
(36) Chaki, N. K.; Negishi, Y.; Tsunoyama, H.; Shichibu, Y.; Tsukuda, T. Ubiquitous 8 and 29 kDa Gold:Alkanethiolate Cluster Compounds: Mass-Spectrometric Determination of Molecular Formulas and Structural Implications. *J. Am. Chem. Soc.* **2008**, *130*, 8608−8610.
(37) Citrin, P. H.; Wertheim, G. K.; Baer, Y. Surface-Atom X-ray Photoemission from Clean Metals: Cu, Ag, and Au. *Phys. Rev. B* **1983**, *27*, 3160−3175.
(38) Wertheim, G. K.; DiCenzo, S. B.; Youngquist, S. E. Unit Charge on Supported Gold Clusters in Photoemission Final State. *Phys. Rev. Lett.* **1983**, *51*, 2310−2313.
(39) Howard, A.; Clark, D. N. S.; Mitchel, C. E. J.; Egdell, R. G.; Dhanak, V. R. Initial and Final State Effects in Photoemission from Au Nanoclusters on TiO_2(110). *Surf. Sci.* **2002**, *518*, 210−224.
(40) Seah, M. P.; Dench, W. A. Quantitative Electron Spectroscopy of Surfaces: A Standard Data Base for Electron Inelastic Mean Free Paths in Solids. *Surf. Interface Anal.* **1979**, *1*, 2−11.
(41) Clay, W. A.; Liu, Z.; Yang, W.; Fabbri, J. D.; Dahl, J. E.; Carlson, R. M. K.; Sun, Y.; Schreiner, P. R.; Fokin, A. A.; Tkachenko, B. A.; et al. Origin of the Monochromatic Photoemission Peak in Diamondoid Monolayers. *Nano Lett.* **2009**, *9*, 57−61.
(42) Zhu, Y.; Jin, R.; Sun, Y. Atomically Monodisperse Gold Nanoclusters Catalysts with Precise Core-Shell Structure. *Catalysts* **2011**, *1*, 3−17.
(43) Bzowski, A.; Sham, T. K.; Watson, R. E.; M. Weinert, M. Electronic Structure of Au and Ag Overlayers on Ru(001): The Behavior of the Noble-Metal *d* Bands. *Phys. Rev. B* **1995**, *51*, 9979−9984.
(44) Sham, T. K.; Yiu, Y. M.; Kuhn, M.; Tan, K. H. Electronic Structure of Ordered and Disordered Cu, Au: The Behavior of the Au 5*d* Bands. *Phys. Rev. B* **1990**, *41*, 11881−11886.
(45) Pirkkalainen, K.; Serimaa, R. Coordination Number in Ideal Spherical Nanocrystals. *J. Appl. Crystallogr.* **2009**, *42*, 442−447.
(46) Ohyama, J.; Teramura, K.; Shishido, T.; Hitomi, Y.; Kato, K.; Tanida, H.; Uruga, T.; Tanaka, T. In Situ Au L_3 and L_2 Edge XANES Spectral Analysis during Growth of Thiol Protected Gold Nanoparticles for the Study on Particle Size Dependent Electronic Properties. *Chem. Phys. Lett.* **2011**, *507*, 105−110.
(47) Park, Y. S.; Whalley, A. C.; Kamenetska, M.; Steigerwald, M. L.; Hybertsen, M. S.; Nuckolls, C.; Venkataraman, L. Contact Chemistry and Single-Molecule Conductance: A Comparison of Phosphines, Methyl Sulfides, And Amines. *J. Am. Chem. Soc.* **2007**, *129*, 15768−15769.
(48) Lopez-Acevedo, O.; Clayborne, P. A.; Häkkinen, H. Electronic Structure of Gold, Aluminum, And Gallium Superatom Complexes. *Phys. Rev. B* **2011**, *84*, 035434.
(49) Akola, J.; Kacprzak, K. A.; Lopez-Acevedo, O.; Walter, M.; Grönbeck, H.; Häkkinen, H. Thiolate-Protected Au_{25} Superatoms as Building Blocks: Dimers and Crystals. *J. Phys. Chem. C* **2010**, *114*, 15986−15994.
(50) Lopez-Acevedo, O.; Tsunoyama, H.; Tsukuda, T.; Häkkinen, H.; Aikens, C. M. Chirality and Electronic Structure of the Thiolate-Protected Au_{38} Nanocluster. *J. Am. Chem. Soc.* **2010**, *132*, 8210−8218.
(51) Akola, J.; Walter, M.; Whetten, R. L.; Häkkinen, H.; Grönbeck, H. On the Structure of Thiolate-Protected Au_{25}. *J. Am. Chem. Soc.* **2008**, *130*, 3756−3757.
(52) Aikens, C. M. Geometric and Electronic Structure of $Au_{25}(SphX)_{18}^-$ (X = H, F, Cl, Br, CH_3, and OCH_3). *J. Phys. Chem. Lett.* **2010**, *1*, 2594−2599.
(53) Aikens, C. M. Effects of Core Distances, Solvent, Ligand, and Level of Theory on the TDDFT Optical Absorption Spectrum of Thiolate-Protected Au_{25} Nanoparticle. *J. Phys. Chem. A* **2009**, *113*, 10811−10817.
(54) Chevrier, D. M.; MacDonald, M. A.; Chatt, A.; Zhang, P.; Wu, Z.; Jin, R. Sensitivity of Structural and Electronic Properties of Gold-Thiolate Nanoclusters to the Atomic Composition: A Comparative X-ray Study of $Au_{19}(SR)_{13}$ and $Au_{25}(SR)_{18}$. *J. Phys. Chem. C* **2012**, *116*, 25137−25142.
(55) Pei, Y.; Gao, Y.; Zeng, X. C. Structural Prediction of Thiolate-Protected Au_{38}: A Face-Fused Bi-Icosahedral Au Core. *J. Am. Chem. Soc.* **2008**, *130*, 7830−7832.
(56) MacDonald, M. A.; Zhang, P.; Chen, N.; Qian, H.; Jin, R. Solution-Phase Structure and Bonding of $Au_{38}(SR)_{24}$ Nanoclusters from X-ray Absorption Spectroscopy. *J. Phys. Chem. C* **2011**, *115*, 65−69.